Adsorption (2023) 29:45–64
https://doi.org/10.1007/s10450-023-00379-x

Estimation of isosteric heat of adsorption from generalized Langmuir isotherm

Usman Hamid[1] · **Pradeep Vyawahare**[1] · **Chau-Chyun Chen**[1]

Received: 10 July 2022 / Revised: 17 January 2023 / Accepted: 19 January 2023 / Published online: 30 January 2023

Abstract
Simulation and design of adsorptive separation units demand accurate estimation of thermodynamic properties. Isosteric heat of adsorption as calculated from generalized Langmuir (gL) isotherm coupled with Clausius–Clapeyron expression for pure component and mixed-gas adsorption equilibria is presented in this work. The estimated isosteric heat of adsorption as functions of surface loading and composition is validated against the experimental data for various adsorption systems. Furthermore, the gL results are compared against classical Langmuir (cL) and Toth isotherm for pure components and with Ideal Adsorbed Solution Theory (IAST) for mixed-gas adsorption equilibria. The comparison highlights that gL outperforms cL and Toth for pure component adsorption and IAST for mixed-gas adsorption, and gL reliably captures the loading dependence and the composition dependence for isosteric heat of adsorption.

Keywords aNRTL activity coefficient model · Classical Langmuir isotherm · Generalized Langmuir isotherm · Ideal adsorbed solution theory · Isosteric heat of adsorption · Toth isotherm

1 Introduction

Accurate process simulation of adsorption systems is instrumental for development and implementation of adsorptive separations such as pressure and temperature swing adsorption units [1, 2]. However, accurate simulation of adsorption systems requires reliable data and rigorous thermodynamic models to describe pure component adsorption isotherms, to estimate mixed-gas adsorption equilibria, and to calculate isosteric heat of adsorption [3].

In general, isosteric heat of adsorption remains constant for homogenous adsorbents and decreases with an increase in surface loading for heterogeneous adsorbents [4]. It can be obtained either from direct measurements using calorimeter or upon regression of adsorption isotherms over a range of temperature [5]. Although calorimeter measurements are considered more reliable, very few such measurements have been reported in the literature [5–8]. Moreover, there is no experimental heat of adsorption data available for ternary and higher-order gas adsorption systems because of convoluted measurement procedures and diminished accuracy [5, 9–12]. Therefore, it is crucially important to apply rigorous and thermodynamically consistent models to provide reliable estimations for isosteric heat of adsorption for pure and mixed-gas adsorption systems [2, 10].

Isosteric heat of adsorption of single component is often calculated from pure component adsorption isotherm models combined with Clausius–Clapeyron equation [5, 12–14] For instance, Tun and Chen [13] presented a comprehensive study to estimate pure component isosteric heat of adsorption using classical Langmuir (cL) [15], Dual-site Langmuir (DSL) [16], Toth [17], and thermodynamic Langmuir (tL) [18] for various adsorbate–adsorbent systems. Independent of adsorbate loading, cL isotherm is applicable only for energetically homogeneous adsorbents [13, 14]. Requiring excessively large number of adjustable parameters, DSL isotherm suggests two types of energetic sites and shows abnormal loading dependence [13]. Toth isotherm introduces an empirical parameter to address adsorbent surface heterogeneity [14] but it yields an unrealistic trend that the isosteric heat of adsorption should approach negative infinity as the amount adsorbed reaches saturation loading [13]. In contrast, tL outperforms cL, DSL, and Toth while addressing adsorbent surface heterogeneity [13] with adsorption Non-random Two-liquid (aNRTL) activity coefficient model [19].

✉ Chau-Chyun Chen
Chauchyun.Chen@ttu.edu

[1] Department of Chemical Engineering, Texas Tech University, Lubbock, TX 79409-3121, USA

Isosteric heat of adsorption for multicomponent adsorption equilibria remains relatively undeveloped [12]. In the last half-century, a few models and theories have been proposed to calculate isosteric heat of adsorption for multicomponent gas adsorption systems. For instance, Sircar [20] presented a cumbersome procedure based on a Jacobian evaluation of "surface excess" of each adsorbate component in the mixture with respect to temperature, pressure, and composition. However, the evaluation of Jacobian matrix heavily relies on the experimental data which according to the author "could be an experimental nightmare" [21]. Bulow and Lorenz [22] avoided the evaluation of Jacobian matrix and proposed the direct use of Clausius–Clapeyron equation for pure component and mixed-gas adsorption. The experimentally measured variation in pressure for pure component and variation of partial pressure for mixed-gas with respect to temperature can be introduced into Clausius–Clapeyron equation to estimate isosteric heat of adsorption. Although the method appears to be simple but it is only applicable to the homogeneous adsorbents and subject to large inaccuracies at high surface coverage [23]. Siperstein et al. [9] proposed a Margules-based spreading pressure-dependent activity coefficient model to capture the adsorbed phase nonideality in Ideal Adsorbed Solution Theory (IAST) [24] framework to estimate isosteric heat of adsorption, but the underlying Margules parameters lack physical meaning. Later Siperstein and Myers [25] presented another attempt to correlate pure component isotherm using four virial coefficients and the Margules-based spreading pressure-dependent model for mixed-gas adsorption, but empiricism of the model persists. Sundaram and Yang [2] implemented modified Dubinin isotherm [26] with Clausius–Clapeyron equation to estimate pure and mixed-gas isosteric heat of adsorption. However, it requires pore volume, adsorbed phase density, Antoine constants, and a few additional empirical parameters making the overall computation burdensome. In short, models available to-date to estimate isosteric heat of adsorption in multicomponent adsorption equilibria either are computationally cumbersome or involve excessive number of empirical parameters.

Recently, Hamid et al. [27] presented generalized Langmuir (gL) isotherm, a rigorous and thermodynamically consistent generalization of tL isotherm, [18] to represent pure component and multicomponent gas adsorption equilibria. Unlike IAST [24], gL considers adsorbent vacant sites in the thermodynamic modeling of gas adsorption equilibria [27] and addresses both surface heterogeneity and adsorbed phase nonideality with the aNRTL activity coefficient model [19]. The resulting gL isotherm reliably tracks and accounts for both adsorbent surface loading dependence and adsorbed phase composition dependence in multicomponent gas adsorption equilibria. This work presents gL estimations of isosteric heat of adsorption for pure component and multicomponent gas adsorption equilibria. In addition, the gL results are compared against cL and Toth isotherms for single component adsorption and with IAST for mixed-gas adsorption equilibria.

2 Pure component isosteric heat of adsorption

Isosteric heat of adsorption for pure component 1, $Q_{st,1}$, can be determined from adsorption isotherm and Clausius–Clapeyron equation presented as follows [1, 28].

$$Q_{st,1} = RT^2\left(\frac{\partial \ln P}{\partial T}\right)_{n_1} \tag{1}$$

where R, T, and P are the gas constant, the system temperature, and the system pressure, respectively. n_1 is the adsorbed amount of component 1. Equation (1) is then combined with pure component isotherm models including classical Langmuir [15], Toth [17], and gL [27] to compute isosteric heat of adsorption in this work.

2.1 Classical Langmuir isotherm

Classical Langmuir isotherm expression for the pure component adsorption amount of adsorbate component 1, n_1, as a function of the system pressure P is shown in Eq. (2).

$$n_1 = n_1^0 \frac{K_1 P}{1 + K_1 P} \tag{2}$$

where n_1^0 and K_1 are the saturation loading and the apparent adsorption equilibrium constant of adsorbate component 1, respectively. The van't Hoff equation [14] expresses the temperature dependence of the apparent adsorption equilibrium constant, given in Eq. (3).

$$K_1 = K_1^{ref} \exp\left[\frac{-E_1}{R}\left(\frac{1}{T} - \frac{1}{T^{ref}}\right)\right] \tag{3}$$

where K_1^{ref} is the apparent adsorption equilibrium constant at reference temperature, T^{ref}, i.e., 298.15 K; E_1 is the heat of adsorption. After combining Eqs. (1) to (3), $Q_{st,1}$, is obtained as Eq. (4).

$$Q_{st,1}(n_1) = E_1 \tag{4}$$

Equation (4) shows that the heat of adsorption from cL is a constant and independent of surface loading and temperature.

2.2 Toth isotherm

Toth isotherm, shown in Eq. (5), introduces an empirical adsorbent surface heterogeneity factor "f" with a temperature dependence shown in Eq. (6).

$$n_1 = n_1^0 \frac{K_1 P}{\left[1 + \left(K_1 P\right)^f\right]^{1/f}} \tag{5}$$

$$f = f^0 + \frac{\beta}{T} \tag{6}$$

here f^0 and β are empirical parameters. Note that the temperature dependence of the apparent adsorption equilibrium constant, K_1, is same as Eq. (3). Combining Toth isotherm with Clausius–Clapeyron equation results in Eq. (7) for isosteric heat of adsorption.

$$Q_{st,1}\left(n_1, T\right) = E_1 + \frac{\beta R}{f}\left[\ln\left(\frac{n_1/n_1^0}{\left\{1 - \left(n_1/n_1^0\right)^f\right\}^{1/f}}\right) - \frac{\ln\left(n_1/n_1^0\right)}{1 - \left(n_1/n_1^0\right)^f}\right] \tag{7}$$

Equation (7) shows that $Q_{st,1}$ is a function of surface loading and temperature. Toth isotherm would falsely predict negative infinity for $Q_{st,1}$ as the adsorption of adsorbate component 1 approaches the saturation loading, i.e., $n_1 \to n_1^0$ [13].

2.3 Generalized Langmuir isotherm

Considering both adsorbent occupied sites and vacant sites, the pure component gL isotherm expressions for the occupied sites and the vacant sites are given below.

$$\theta_1 = \frac{n_1 A_1}{A^0} = \frac{n_1}{n_1^0} = \frac{K_1^o P}{\frac{\gamma_1}{\gamma_\phi q_1} + K_1^o P} \tag{8}$$

$$\theta_\phi = \frac{n_\phi A_\phi}{A^0} = \frac{n_\phi}{n_\phi^0} = \frac{1}{1 + \frac{\gamma_\phi q_1}{\gamma_1} K_1^o P} \tag{9}$$

$$K_1^o = \frac{x_1 \gamma_1}{x_\phi \gamma_\phi P} \tag{10}$$

$$q_1 = \frac{A_1}{A_\phi} \tag{11}$$

where θ_1 is adsorbed phase area fraction of adsorbate component 1, n_1 is the amount adsorbed, n_1^0 is the saturation loading, A_1 is the effective molar surface area, γ_1 denotes the activity coefficient, and K_1^o represents the intrinsic adsorption equilibrium constant. θ_ϕ is the adsorbed phase area fraction of "phantom" molecule ϕ representing the vacant sites, n_ϕ is the amount adsorbed, n_ϕ^0 is the saturation loading, A_ϕ is the effective molar surface area, and γ_ϕ denotes the activity coefficient. Note that nitrogen molecule is considered as the model "phantom" molecule since it is used to determine the adsorbent surface area, A^0. The activity coefficients can be computed using area-based aNRTL model [27] given as follow:

$$\frac{g^E}{RT} = q_1 \frac{x_1 x_\phi \tau_{1\phi}\left[G_{1\phi} - 1\right]}{\left(x_1 q_1 G_{1\phi} + x_\phi\right)} \tag{12}$$

$$\ln \gamma_1 = q_1 \frac{x_\phi^2 \tau_{1\phi}\left[G_{1\phi} - 1\right]}{\left(x_1 q_1 G_{1\phi} + x_\phi\right)^2} \tag{13}$$

$$\ln \gamma_\phi = \frac{x_1^2 q_1^2 \tau_{\phi 1}\left[G_{\phi 1} - 1\right]}{\left(x_1 q_1 + x_\phi G_{\phi 1}\right)^2} \tag{14}$$

$$\tau_{1\phi} = -\tau_{\phi 1} = \frac{g_{10} - g_{\phi 0}}{RT} \tag{15}$$

$$G_{1\phi} = \exp\left(-\alpha \tau_{1\phi}\right) \tag{16}$$

$$x_1 = \frac{n_1}{n_T} \tag{17}$$

$$x_\phi = \frac{n_\phi}{n_T} \tag{18}$$

$$n_T = n_1 + n_\phi \tag{19}$$

where x_1 and x_ϕ are the adsorbed phase mole fractions of adsorbate component 1 and phantom molecule ϕ, respectively. n_T is the total amount adsorbed. g_{10} and $g_{\phi 0}$ are the interaction energies of adsorbate component 1 and phantom molecule ϕ with adsorbent site "0", respectively. $\tau_{1\phi}$ represents the binary interaction parameter of adsorbate component 1 with phantom molecule ϕ, and α is a non-randomness factor set to 0.3 per the NRTL convention [27, 29]. The temperature dependence of K_1^o and $\tau_{1\phi}$ are as follow:

$$K_1^o = K_1^{o^{ref}} \exp\left[\frac{-E_1}{R}\left(\frac{1}{T} - \frac{1}{T^{ref}}\right)\right] \tag{20}$$

$$\tau_{1\phi} = A_{1\phi} + \frac{B_{1\phi}}{T} \approx \frac{B_{1\phi}}{T} \tag{21}$$

where $K_1^{o^{ref}}$ denotes the intrinsic adsorption equilibrium constant at the reference temperature, T^{ref}, and E_1 is the heat of

adsorption. Note that $\tau_{1\phi}$ requires only the parameter $B_{1\phi}$ to capture the temperature dependence since $A_{1\phi}$ does not improve pure component adsorption isotherm representation. $B_{1\phi}$ has the unit of temperature K. Combining Eq. (1) and gL results in Eq. (22) for the isosteric heat of adsorption.

$$Q_{st,1}\left(n_1,T\right)=E_1+RT^2\left(\frac{\partial \ln \gamma_1}{\partial T}-\frac{\partial \ln \gamma_\phi}{\partial T}\right)_{n_1} \tag{22}$$

here $\frac{\partial \ln \gamma_1}{\partial T}$ and $\frac{\partial \ln \gamma_\phi}{\partial T}$ account for the contributions from the adsorbed phase heterogeneity, i.e., the nonideality due to surface loading. A complete derivation of Eq. (22) is given in Section I of Supplementary Information.

3 Isosteric heat of adsorption in mixed-gas adsorption

Isosteric heat of adsorption of component i in mixed-gas adsorption equilibria, $Q_{st,i}^{mix}$, can be estimated with Clausius–Clapeyron equation as presented in Eq. (23). [1, 23]

$$Q_{st,i}^{mix}=RT^2\left(\frac{\partial \ln Py_i}{\partial T}\right)_{n_i} \tag{23}$$

here y_i is the gas phase mole fraction of adsorbate component i at the system pressure P. The following sections present the thermodynamic formulations with IAST [24] and gL [27] to estimate isosteric heat of adsorption in mixed-gas adsorption equilibria.

3.1 Ideal adsorbed solution Theory

IAST calculates the adsorbed phase mole fraction of component i, x_i', exclusive of adsorbent vacant sites, from a Raoult's law-type equation as shown below.

$$Py_i=x_i'P_i^o(T,\psi) \tag{24}$$

here P_i^o denotes the equilibrium pressure of the adsorbate component i in adsorbed phase calculated at the constant "spreading pressure" constraint, i.e., $\psi_i=\psi_j=\psi_{mix}$ where i and j are the adsorbate species in the mixture. ψ is the hypothetical spreading pressure calculated from the pure component adsorption isotherm, $n_i(P)$, as presented in Eq. (25).

$$\psi_i=\int_0^{P_i^o} n_i(P)d\ln P \tag{25}$$

here $n_i(P)$ is the amount adsorbed as a function of pressure, P, represented with the gL isotherm for pure component adsorption in this study. Upon combining Eqs. (23)–(25), the isosteric heat of adsorption of adsorbate component i can be calculated from Eqs. (26) to (28).

$$Q_{st,i}^{mix}\left(n_i^o,T\right)=\Delta h_i^o+\frac{1}{n_i^o}\left[\frac{\sum_{j=1}^N x_j'F_j^o\cdot n_j^o\left(\Delta\overline{h_j^o}-\Delta h_j^o\right)}{\sum_{j=1}^N x_j'F_j^o}\right] \tag{26}$$

$$\Delta h_i^o=\frac{\int_0^{n_i^o}\Delta\overline{h_i^o}dn_i}{n_i^o} \tag{27}$$

$$F_i^o=\frac{1}{\left(n_i^o\right)^2}\left(\frac{\partial \ln n_i^o}{\partial \ln P_i^o}\right)_T \tag{28}$$

here n_i^o is the adsorption amount and $\Delta\overline{h_i^o}$ is the isosteric heat of adsorption for pure adsorbate component i at equilibrium. Δh_i^o is the integral enthalpy defined by Eq. (27). N represents the total number of adsorbate components. The complete derivation of Eq. (26) can be found elsewhere [25, 30].

3.2 Generalized Langmuir isotherm

The gL isotherm to estimate multicomponent gas adsorption equilibria is given as follow:

$$\theta_i=\frac{n_iA_i}{A^0}=\frac{n_i}{n_i^0}=\frac{K_i^oy_iP}{\frac{\gamma_i}{\gamma_\phi q_i}+\sum_{j=1}^N\frac{\gamma_iq_j}{\gamma_jq_i}K_j^oy_jP} \tag{29}$$

$$\theta_\phi=\frac{n_\phi A_\phi}{A^0}=\frac{n_\phi}{n_\phi^0}=\frac{1}{1+\sum_{j=1}^N\frac{\gamma_\phi q_j}{\gamma_j}K_j^oy_jP} \tag{30}$$

$$K_i^o=\frac{x_i\gamma_i}{x_\phi\gamma_\phi Py_i} \tag{31}$$

$$q_i=\frac{A_i}{A_\phi} \tag{32}$$

$$A^0=\sum_{i=1}^N n_iA_i+n_\phi A_\phi=n_i^0A_i=n_\phi^0A_\phi \tag{33}$$

where y_i is the gas phase mole fraction of adsorbate component i, θ_i is the adsorbed phase area fraction, n_i is the adsorption amount, n_i^0 is the adsorption saturation loading, and γ_i is the activity coefficient. θ_ϕ is the adsorbed phase area

fraction of "phantom" molecule ϕ, n_ϕ is the adsorption amount, n_ϕ^0 is the adsorption saturation loading, and γ_ϕ is the activity coefficient. A^0 is the constant adsorbent surface area. It is worth noting again that gL treats the adsorbent vacant sites as an integral part of the adsorptive system. Therefore, single component gas adsorption is treated as a binary system involving one adsorbate component for the occupied sites and one phantom molecule ϕ component for the vacant sites. Similarly, binary gas adsorption is treated as a ternary system having two adsorbate components for the occupied sites and one phantom molecule ϕ component for the vacant sites. Activity coefficients for the multicomponent adsorbed phase can be computed from the area-based aNRTL activity coefficient model, given as follow.

$$\frac{g^E}{RT} = \sum_{i=1}^{M} x_i q_i \frac{\sum_{j=1}^{M} x_j q_j \tau_{ij}}{\sum_{k=1}^{M} x_k q_k G_{ki}} \tag{34}$$

$$\ln \gamma_i = q_i \sum_{j=1}^{M} \frac{x_j^2 q_j^2 \tau_{ij} \left[G_{ij} - 1\right]}{\left(\sum_{k=1}^{M} x_k q_k G_{kj}\right)^2} \tag{35}$$

$$\tau_{ij} = -\tau_{ji} = \frac{g_{i0} - g_{j0}}{RT} \tag{36}$$

$$G_{ij} = \exp\left(-\alpha \tau_{ij}\right) \tag{37}$$

$$x_i = \frac{n_i}{n_T} \tag{38}$$

$$x_\phi = \frac{n_\phi}{n_T} \tag{39}$$

$$n_T = \sum_{i=1}^{N} n_i + n_\phi \tag{40}$$

here τ_{ij} is the binary interaction parameter for the adsorbate i—adsorbate j interaction. x_i and x_ϕ are the adsorbed phase mole fractions of adsorbate component i and phantom molecule ϕ, respectively. M is the total number of adsorbates, N, plus one for phantom molecule ϕ. The temperature dependence of the intrinsic adsorption equilibrium constant, K_i^o, and that of the binary interaction parameter, τ_{ij}, are same as Eqs. (20) and (21) for the pure component gL isotherm.

A general expression to estimate the isosteric heat of adsorption of adsorbate component i in the adsorption mixture is given in Eq. (41):

$$Q_{st,i}(n_i) = E_i + RT^2 \left[\frac{\partial \ln \gamma_i}{\partial T} - \frac{\partial \ln \gamma_\phi}{\partial T}\right]_{n_i} \tag{41}$$

where $\frac{\partial \ln \gamma_i}{\partial T}$ and $\frac{\partial \ln \gamma_\phi}{\partial T}$ account for the contributions from the nonidealities due to adsorbed phase loading and composition. A complete derivation of the isosteric heat of adsorption for binary mixed-gas adsorption is given in Section II of Supplementary Information.

4 Results and discussion

This section first presents the generalized Langmuir isotherm estimations for pure component isosteric heat of adsorption along with the results from the classical Langmuir and Toth isotherms. The "predictive" approach estimates the isosteric heat of adsorption based on pure component isotherm data over a range of temperatures. The "correlative" approach estimates the isosteric heat of adsorption based on simultaneous regression of pure component adsorption isotherm and isosteric heat of adsorption data at a specific temperature.

This section then presents the generalized Langmuir isotherm estimations for isosteric heat of adsorption of each component in binary adsorption mixtures. The gL results for isosteric heat of adsorption are further compared against the Ideal Adsorbed Solution Theory predictions to highlight the effects of surface loading and adsorbed phase composition.

4.1 "Predictive" pure component isosteric heat of adsorption

Accurate representation of pure component adsorption isotherms over a wide temperature range forms a solid foundation to estimate isosteric heat of adsorption. Classical Langmuir, Toth, and generalized Langmuir isotherms are used in this work to correlate experimental pure component adsorption isotherms and predict isosteric heat of adsorption. cL requires three parameters, i.e., n_i^0, K_i^{ref}, and E_i while Toth requires five model parameters, i.e., n_i^0, K_i^{ref}, E_i, f^0, and β. In contrast, with literature reported values for A^0 and A_i to calculate n_i^0, gL requires only three adjustable parameters, i.e., $K_i^{o^{ref}}$, E_i, and $B_{i\phi}$.

The objective function minimized to identify the adsorption isotherm parameters is based on the Maximum Likelihood Principle [31], given as follows:

Table 1 Model parameters for classical Langmuir isotherm

Adsorbent	Adsorbate	T (K)	n_i^0 (mol/kg)	K_i^{ref} (bar^{-1})	E_i (kJ/mol)	n_i RMSE (mol/kg)	$Q_{st,i}$ ARD%
Zeolite 13X[a] [14, 32]	CO_2	273.15–473.15	5.10 ± 0.01	40.754 ± 0.094	36.52 ± 0.07	0.358	6.25
Nuxit-AL charcoal[a] [2, 33]	CH_4	293.1–363.1	3.06 ± 0.03	0.316 ± 0.011	18.64 ± 2.74	0.017	–
	C_2H_4	293.1–363.1	4.48 ± 0.01	1.751 ± 0.029	25.45 ± 0.04	0.128	–
Silicalite[b] [6]	O_2	305.45	1.83 ± 8.00	0.103 ± 0.483	16.33 ± 0.28	0.000	3.29
	N_2	296.1	1.46 ± 3.15	0.154 ± 0.370	17.70 ± 0.29	0.000	2.82
	Ar	305.75	2.31 ± 9.40	0.088 ± 0.378	15.82 ± 0.24	0.000	2.88
	CO_2	303.75	2.62 ± 0.14	1.773 ± 0.159	27.72 ± 0.35	0.010	0.92
	CH_4	296.22	2.28 ± 0.49	0.398 ± 0.111	21.14 ± 0.25	0.001	1.33
	C_2H_6	296.18	2.14 ± 0.02	10.578 ± 0.339	31.77 ± 0.28	0.010	1.36
Zeolite MFI[b] [10]	CH_4	296.2	2.44 ± 0.56	0.365 ± 0.109	21.72 ± 0.37	0.001	2.10
	SF_6	297	1.93 ± 0.01	20.125 ± 0.681	37.22 ± 0.40	0.008	2.93
BPL activated carbon[b] [21]	CH_4	297	2.04 ± 0.36	0.600 ± 0.148	21.28 ± 0.32	0.004	3.67
	C_2H_6	297	3.28 ± 0.03	4.962 ± 0.104	28.80 ± 0.19	0.096	6.38
NaX[b] [8]	CO_2	305.95	4.62 ± 0.02	70.884 ± 1.699	39.29 ± 0.42	0.253	6.95
	C_2H_6	305.55	4.79 ± 0.18	3.782 ± 0.302	30.01 ± 0.33	0.068	6.87

[a]Parameter regression using adsorption isotherms at multiple temperatures

[b]Parameter regression using adsorption isotherm and isosteric heat of adsorption data

$$Obj = \sum_{l}^{N} \left(\frac{n_l^{calc} - n_l^{expt}}{\sigma_{n_l^{expt}}} \right)^2 \tag{42}$$

where l is the data point index, N is the total number of data points, and n_l^{calc} and n_l^{expt} indicate the calculated and the experimental amounts adsorbed. $\sigma_{n_l^{expt}}$ is the standard deviation of the experimental data with a default value set to 0.05 mol/kg. Root Mean Square Error (RMSE) and Average Relative Deviation (ARD%) have been calculated to compare the goodness of fit for pure component adsorption isotherm and isosteric heat of adsorption, expressed below:

$$RMSE = \sqrt{\frac{\sum_{l=1}^{N} \left(n_l^{calc} - n_l^{expt} \right)^2}{N}} \tag{43}$$

$$ARD\% = \frac{100}{N} \sum_{l=1}^{N} \left| \frac{Q_{st,l}^{calc} - Q_{st,l}^{expt}}{Q_{st,l}^{expt}} \right| \tag{44}$$

$Q_{st,l}^{calc}$ and $Q_{st,l}^{expt}$ are the calculated and the measured isosteric heat of adsorption, respectively.

Three pure component adsorption isotherm data sets are selected to illustrate the predictions of isosteric heat of adsorption from pure component adsorption isotherms: (1) CO_2 adsorption on Zeolite 13X at 273.15–473.15 K, [14, 32], (2) CH_4, and (3) C_2H_4 adsorption on Nuxit-AL charcoal at 293.1–363.1 K [2, 33]. The regression parameters, RMSE's, and ARD%'s of cL, Toth, and gL are presented in Tables 1, 2, and 3, respectively.

Figure 1 shows the Log–Log graphical illustration of the CO_2 adsorption isotherm data on Zeolite 13X [14, 32]. Figure 1a shows cL model fitting fails to represent the CO_2 adsorption isotherm data on Zeolite 13X with three adjustable parameters for the entire temperature range of 273.15–473.15 K. Although Toth fits the low temperatures isotherm data reasonably well with five adjustable parameters, Fig. 1b shows the fit deviates significantly at temperatures above 398.15 K. On the other hand, with the exception of pressures less than 10 Pa, gL reliably captures the experimental data with three adjustable parameters for the whole range of temperatures and pressures as shown in Fig. 1c. Note that, with the default value of 0.05 mol/kg for the standard deviation of the adsorption amount data, the adsorption isotherm data of CO_2 on Zeolite 13X at low pressures are assumed to be subject to higher uncertainties.

Son et al. [14] reported comprehensive heat of adsorption data as a function of CO_2 loading on Zeolite 13X at different temperatures using a differential scanning calorimeter. To evaluate the performance of each model, we predict the isosteric heat of adsorption based on the parameters regressed from pure component adsorption isotherm data as shown in Tables 1, 2, and 3. Figure 2a shows that cL predicts a constant isosteric heat of adsorption that is inconsistent with the experimental data. Figure 2b shows the Toth predictions are significantly too high although the decreasing trend w.r.t. the loading is consistent with the data. In contrast, the gL predictions fall in the range of the experimental heat of adsorption data as shown in Fig. 2c. Figure 2c further shows that gL predicts, at low loadings, the heat of adsorption should

Table 2 Model parameters for Toth isotherm

Adsorbent	Adsorbate	T (K)	n_i^0 (mol/kg)	K_i^{ref} (bar^{-1})	E_i (kJ/mol)	f^0	β(K)	n_i RMSE (mol/kg)	$Q_{st,i}$ ARD%
Zeolite 13X[a] [14, 32]	CO_2	273.15–473.15	7.55 ± 0	694.736 ± 0.083	47.54 ± 0.12	0.48 ± 0	− 49.65 ± 0.16	0.067	4.79
Nuxit-AL charcoal[a] [2, 33]	CH_4	293.1–363.1	7.48 ± 0.01	0.179 ± 0	20.83 ± 0.01	0.88 ± 0	− 99.77 ± 0.12	0.012	–
	C_2H_4	293.1–363.1	10.56 ± 0.23	3.424 ± 0.016	31.61 ± 0.72	0.60 ± 0.02	− 69.01 ± 5.83	0.027	–
Silicalite[b] [6]	O_2	305.45	2.56 ± 10.77	0.074 ± 0.364	16.33 ± 0.45	0.90 ± 3.34	0	0.000	3.29
	N_2	296.1	1.76 ± 189.9	0.129 ± 13.425	17.70 ± 1.36	0.93 ± 37.81	0	0.000	2.82
	Ar	305.75	3.44 ± 13.52	0.060 ± 0.285	15.82 ± 1.69	0.89 ± 1.85	0	0.000	2.88
	CO_2	303.75	4.82 ± 3.42	1.239 ± 0.699	27.72 ± 0.37	0.63 ± 0.35	0	0.001	0.92
	CH_4	296.22	2.43 ± 5.90	0.376 ± 0.821	21.14 ± 0.78	0.96 ± 1.12	0	0.001	1.33
	C_2H_6	296.18	2.14 ± 0.07	10.578 ± 0.512	31.77 ± 0.53	1.00 ± 0.14	0	0.010	1.36
Zeolite MFI[b] [10]	CH_4	296.2	2.91 ± 6.86	0.314 ± 0.654	21.72 ± 0.74	0.90 ± 1.35	0	0.001	2.10
	SF_6	297	1.95 ± 0.04	21.014 ± 2.839	37.22 ± 4.66	0.96 ± 0.41	0	0.007	2.93
BPL activated carbon[b] [21]	CH_4	297	7.07 ± 19.38	0.220 ± 0.483	23.96 ± 1.87	1.00 ± 1.27	− 140.43 ± 217.2	0.001	1.39
	C_2H_6	297	24.20 ± 7.22	6.566 ± 0.427	39.18 ± 1.39	0.43 ± 0.05	− 56.62 ± 8.92	0.009	1.61
NaX[b] [8]	CO_2	305.95	11.42 ± 1.03	670.275 ± 133.808	56.62 ± 2.56	0.54 ± 0.05	− 80.37 ± 12.01	0.027	1.55
	C_2H_6	305.55	4.79 ± 0.90	3.782 ± 5.861	30.01 ± 56.09	1.00 ± 1.86	0	0.060	6.87

[a]Parameter regression using adsorption isotherms at multiple temperatures

[b]Parameter regression using adsorption isotherm and isosteric heat of adsorption data

Table 3 Model parameters for generalized Langmuir isotherm

Adsorbent	Adsorbate	T (K)	n_i^0 (mol/kg)	$K_i^{o^{ref}}$(bar^{-1})	E_i (kJ/mol)	$B_{i\phi}$(K)	A_i (nm^2)	n_i RMSE (mol/kg)	$Q_{st,i}$ ARD%
Zeolite 13X[b] [14, 32]	CO_2	273.15–473.15	5.91 ± 0.02	28.766 ± 0.454	38.08 ± 0.11	− 767.13 ± 2.12	0.163 [40]	0.089	5.11
Nuxit-AL charcoal[b] [2, 33]	CH_4	293.1–363.1	9.46[a]	0.029 ± 0.008	13.54 ± 0.78	− 543.94 ± 29.53	0.166 [41]	0.014	–
	C_2H_4	293.1–363.1	6.98 ± 0.29	0.375 ± 0.045	23.69 ± 0.33	− 518.04 ± 14.25	0.225 [42]	0.029	–
Silicalite[c] [6]	O_2	305.45	3.18[a]	0.066 ± 0.022	16.33 ± 0.28	0	0.141 [40]	0.000	3.29
	N_2	296.1	2.77*	0.077 ± 0.029	17.70 ± 0.30	0	0.162 [40]	0.002	2.82
	Ar	305.75	3.25[a]	0.073 ± 0.024	15.82 ± 0.29	0	0.138 [40]	0.001	2.88
	CO_2	303.75	2.75[a]	1.602 ± 1.077	27.62 ± 0.66	− 133.93 ± 324.72	0.163 [40]	0.009	1.10
	CH_4	296.22	2.70[a]	0.305 ± 0.160	20.95 ± 0.66	− 120.59 ± 232.02	0.166 [41]	0.002	1.40
	C_2H_6	296.18	2.19[a]	7.822 ± 9.815	31.76 ± 0.31	− 88.26 ± 1754.9	0.205 [41]	0.015	1.49
Zeolite MFI[c] [10]	CH_4	296.2	2.67[a]	0.316 ± 0.218	21.67 ± 1.25	− 61.12 ± 940.12	0.166 [41]	0.003	2.10
	SF_6	297	1.93[a]	14.131 ± 22.864	37.22 ± 0.98	− 0.18 ± 142.93	0.230 [41]	0.008	2.93
BPL activated carbon[c] [21]	CH_4	297	10.61[a]	0.020 ± 0.007	12.67 ± 1.73	− 606.77 ± 48.96	0.166 [41]	0.002	1.35
	C_2H_6	297	6.8 [a]	0.449 ± 0.152	23.38 ± 2.48	− 502.10 ± 8.50	0.259 [41]	0.028	2.95
NaX[c] [8]	CO_2	305.95	6.34 ± 0.22	28.961 ± 3.405	39.24 ± 0.47	− 689.53 ± 19.83	0.163 [40]	0.021	0.66
	C_2H_6	305.55	5.04[a]	2.697 ± 1.164	30.00 ± 0.64	− 39.95 ± 1009.54	0.205 [41]	0.074	6.91

[a]Amount adsorbed calculated from A^0

[b]Parameter regression using adsorption isotherms at multiple temperatures

[c]Parameter regression using adsorption isotherm and isosteric heat of adsorption data

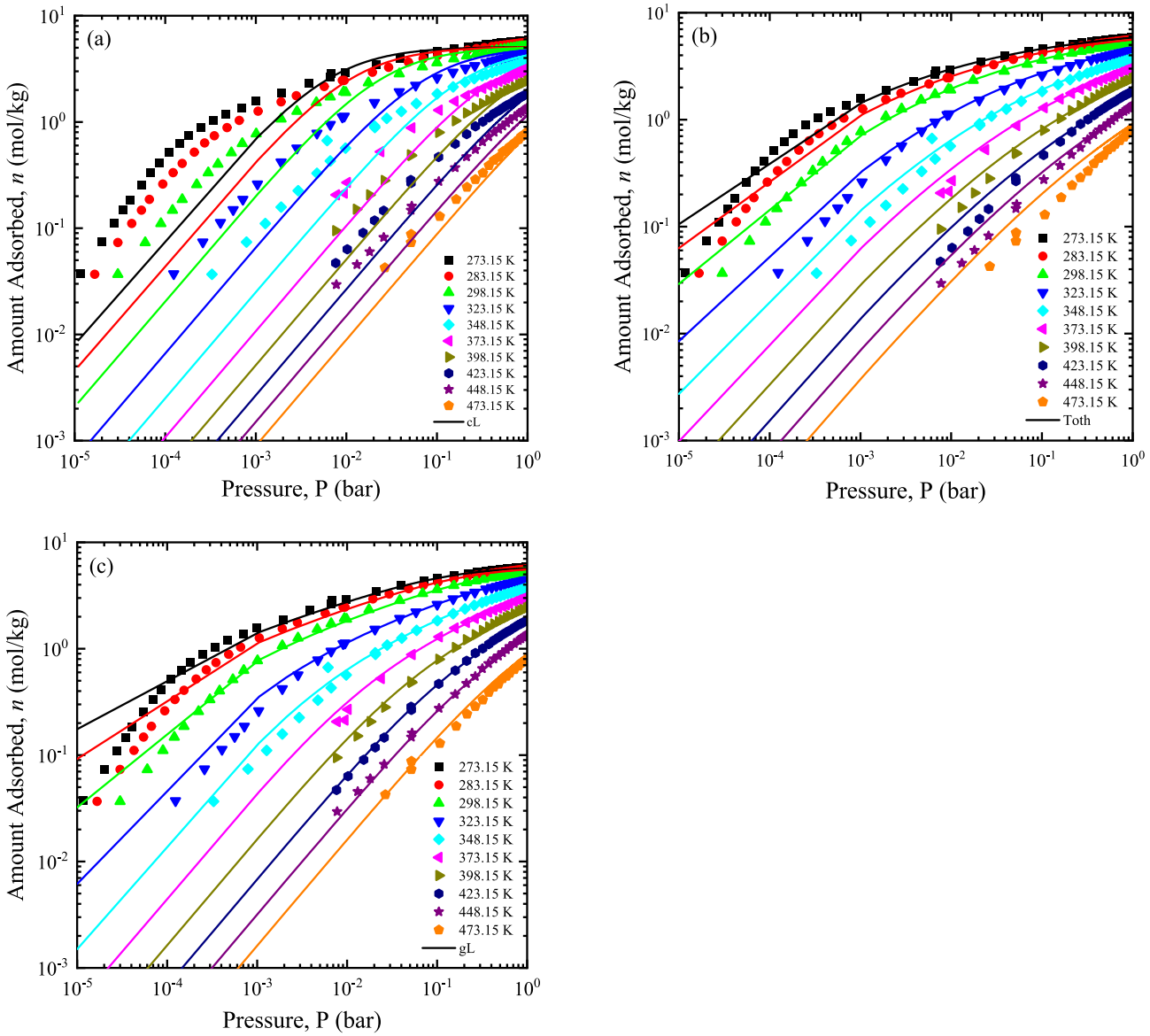

Fig. 1 CO_2 adsorption isotherm on Zeolite 13X at 273.15–473.15 K [14, 32]. **a** Classical Langmuir Log–Log plot, **b** Toth Log–Log plot, and **c** generalized Langmuir Log–Log plot; symbols show the experimental data at a specific temperature

be higher at lower temperatures and, at high loadings, the heat of adsorption would be lower at lower temperatures. This model behavior has been reported for thermodynamic Langmuir isotherm and explained based on Eq. (22) and the temperature dependence of the activity coefficients as suggested by the aNRTL activity coefficient model [13]. We followed Son et al. [14] and excluded the experimental data points at low loadings from Fig. 2 due to associated high data uncertainty.

Similar model behaviors are observed for CH_4 and C_2H_4 adsorption on Nuxit-AL charcoal at 293.1–363.1 K [2, 33]. Figure 3a show that cL, Toth, and gL all reliably capture the experimental CH_4 adsorption isotherm data at all temperatures and pressures. In the case of C_2H_4 adsorption, Toth and gL accurately fit the experimental isotherm data while cL deviates significantly in the low-pressure region as shown in Fig. 3b. Since there are no experimental isosteric heat of adsorption data available for CH_4 and C_2H_4 adsorption on Nuxit-AL charcoal, Fig. 4 shows only the model predictions for isosteric heat

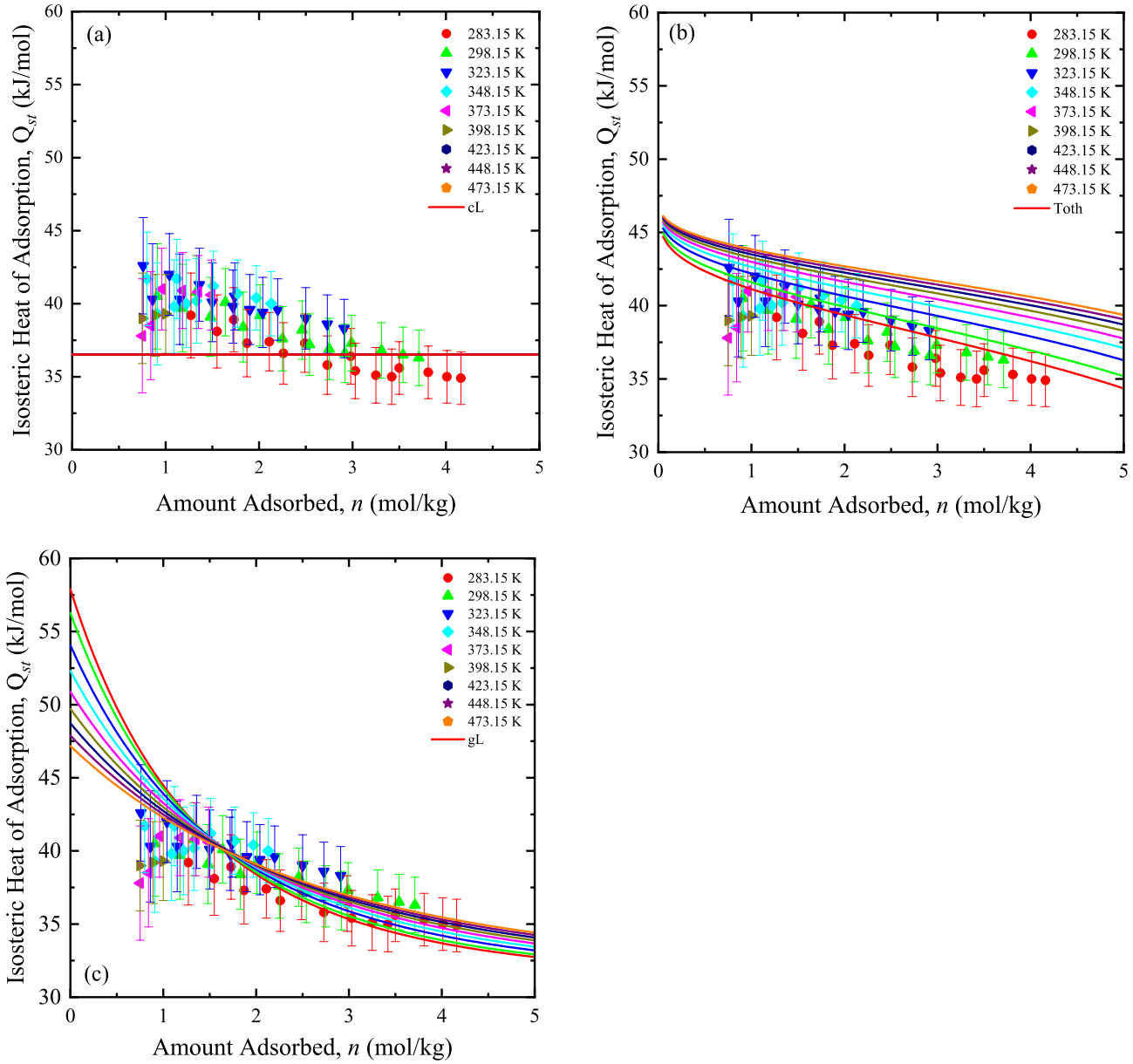

Fig. 2 Isosteric heat of adsorption of CO_2 on Zeolite 13X at 283.15–473.15 K [14, 32]. **a** Classical Langmuir, **b** Toth, and **c** generalized Langmuir; symbols show experimental data with bars indicating the standard deviation

of adsorption from cL, Toth, and gL. Note that all the model predictions are consistent with the observation reported for typical microporous adsorbents [5, 34, 35] that the isosteric heat of adsorption should either remain constant or decrease with the loading.

4.2 "Correlative" pure component isosteric heat of adsorption

Comprehensive adsorption isotherm data covering a wide temperature range is rarely available in the literature to support identification of the isotherm model parameters required to predict isosteric heat of adsorption over the temperature range of interest. An alternative approach is to identify the model parameters from simultaneous regression of available adsorption isotherm and heat of adsorption data. The objective function minimized in this case is given in Eq. (45).

$$Obj = \sum_{l=1}^{N}\left(\frac{n_l^{calc} - n_l^{expt}}{\sigma_{n_l^{expt}}}\right)^2 + \sum_{l=1}^{N'}\left(\frac{Q_{st,l}^{calc} - Q_{st,l}^{expt}}{\sigma_{Q_{st,l}^{expt}}}\right)^2 \quad (45)$$

where N and N' denote the total number of data points in adsorption isotherm and isosteric heat of adsorption

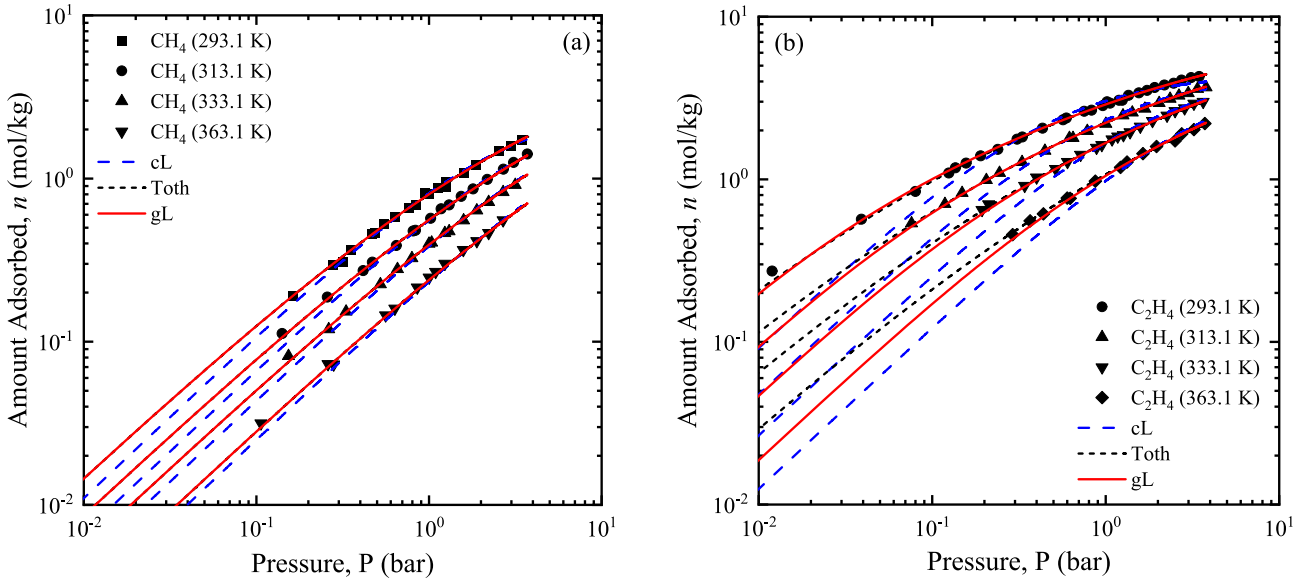

Fig. 3 Adsorption isotherm on Nuxit-AL charcoal at 293.1–363.1 K [2, 33]. **a** CH_4 Log–Log plot and **b** C_2H_4 Log–Log plot

datasets, respectively; $\sigma_{Q_{st,i}^{expt}}$ is the standard deviation of the experimental heat of adsorption set to 2.0 kJ/mol.

The adsorption data of seven different adsorbates on four adsorbents have been examined. These adsorbate–adsorbent systems are O_2 at 305.45 K, N_2 at 296.10 K, Ar at 305.75 K, CO_2 at 303.75 K, CH_4 at 296.22 K, and C_2H_6 at 296.18 K on Silicalite [6], CH_4 at 296.2 K and SF_6 at 297 K on Zeolite MFI [10], CH_4 at 297 K and C_2H_6 at 297 K on BPL Activated Carbon [21], and CO_2 at 305.95 K and C_2H_6 at 305.55 K on NaX [8]. The experimental amount adsorbed and isosteric heat of adsorption datasets were regressed simultaneously to identify the model parameters. The identified model parameters of cL, Toth, and gL along with the RMSE's and ARD%'s are reported in Tables 1, 2, and 3, respectively.

Figure 5a shows the adsorption isotherms of O_2 at 305.45 K, N_2 at 296.10 K, and Ar at 305.75 on Silicalite are well captured with the three isotherm models at all loadings. The heat of adsorption data and the model results presented in Fig. 6a suggest the energetically homogeneous adsorbent surface of Silicalite. Similarly, Figs. 5b and 6b show the data and the model results for the experimental adsorption isotherm and isosteric heat of adsorption of CO_2 at 303.75 K, CH_4 at 296.22 K, and C_2H_6 at 296.18 K on Silicalite. Note that, regardless of the small root mean square errors from the Toth isotherm fitting, the regressed pure component parameters for O_2, N_2, Ar, and CH_4 have very higher uncertainties. With the saturation loading calculated from the adsorbent surface area and the effective area of the adsorbate component, gL offers accurate results with reduced uncertainties in pure component isotherm parameters.

Likewise, cL, Toth, and gL capture the adsorption isotherms of CH_4 at 296.2 K and SF_6 at 297 K on Zeolite MFI at all loadings as shown in Fig. 5c. Figure 6c show that the experimental isosteric heat of adsorption of SF_6 increases with the loading depicting an abnormal behavior. All three models predict that the isosteric heat of adsorption for both adsorbate components should be independent of the surface loading. Note that, other literature reported constant isosteric heat of adsorption of SF_6 on Zeolite MFI [36, 37].

Figure 5d shows the adsorption isotherm data and the model results for CH_4 at 297 K and C_2H_6 at 297 K on BPL activated carbon. While the three models accurately capture the experimental adsorption data of CH_4, their representations for the C_2H_6 adsorption on BPL activated carbon at the low pressures are different. Both cL and gL correctly suggest the Henry's law behavior for the C_2H_6 adsorption at low pressures. However, the cL results are significantly lower than the experimental adsorption data. On the other hand, Toth provides slightly better fitting at the expense of questionable model parameter values. Specifically, the regressed Toth isotherm parameters, i.e., n_i^0, K_i^{ref}, f^0 and β for CH_4 are subject to very high uncertainties and the regressed n_i^0 for C_2H_6 seems exceedingly high. Table 2 shows that the saturation loading of C_2H_6 from Toth would be more than three times the saturation

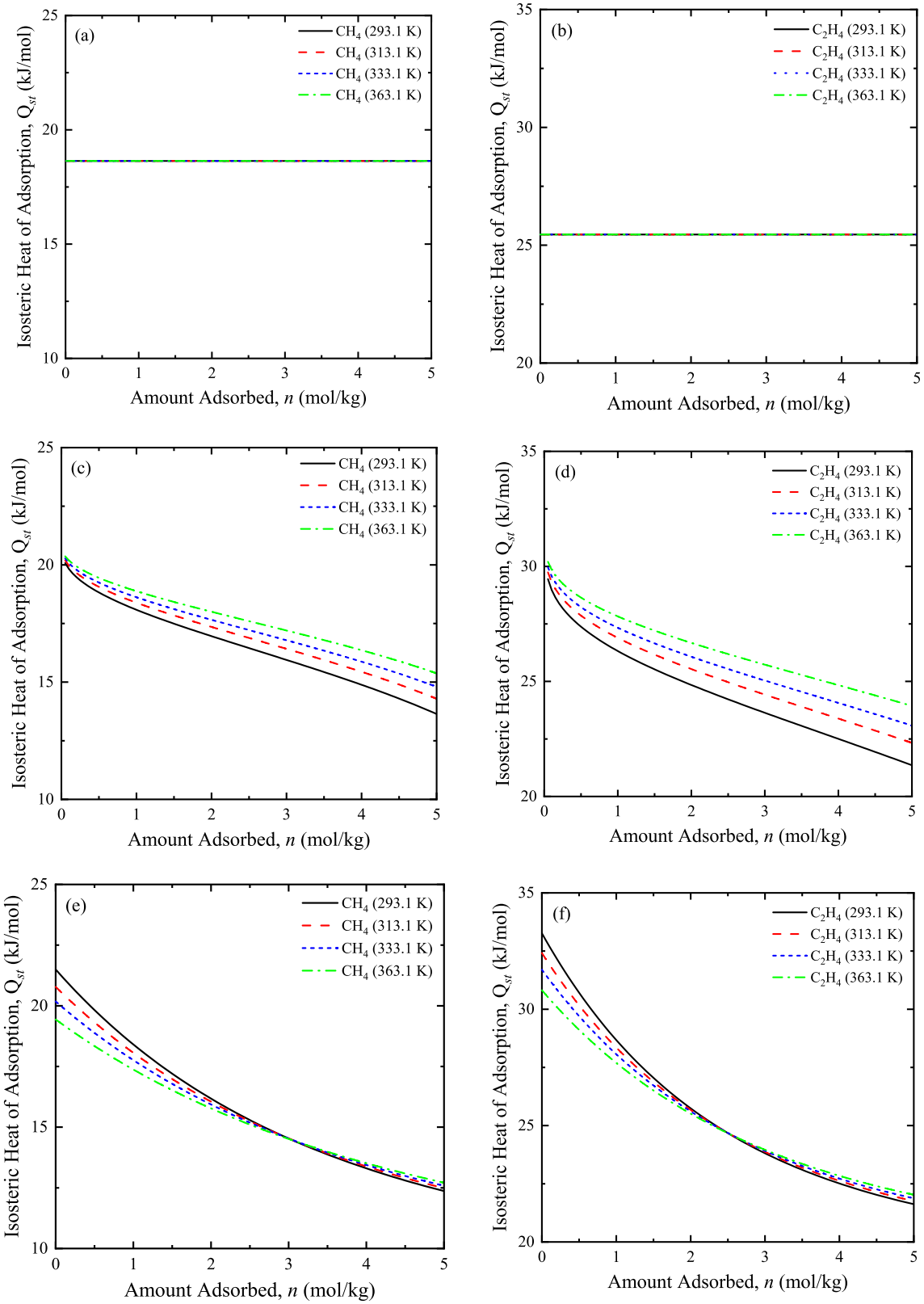

Fig. 4 Isosteric heat of adsorption on Nuxit-AL charcoal at 293.1–363.1 K [2, 33] of **a** CH_4 using classical Langmuir, **b** C_2H_4 using classical Langmuir, **c** CH_4 using Toth, **d** C_2H_4 using Toth, **e** CH_4 using generalized Langmuir, and **f** C_2H_4 using generalized Langmuir

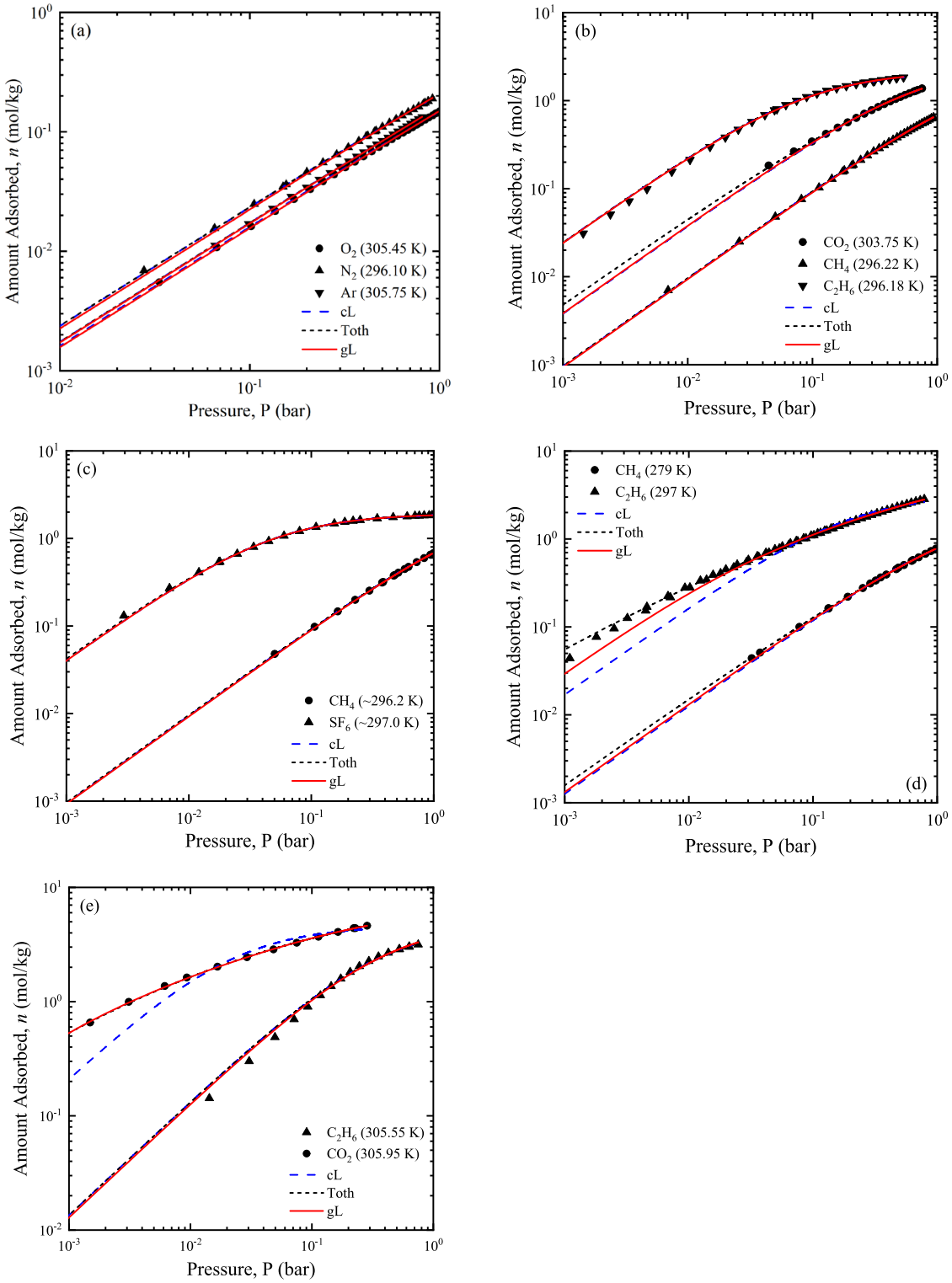

Fig. 5 Pure component adsorption isotherm of **a** O_2 at 305.45 K, N_2 at 296.10 K, and Ar at 305.75 K on Silicalite [6] Log–Log plot, **b** CO_2 at 303.75 K, CH_4 at 296.22 K, and C_2H_6 at 296.18 K on Silicalite [6] Log–Log plot, **c** CH_4 at 296.2 K and SF_6 at 297.0 K on Zeolite MFI [10] Log–Log plot **d** CH_4 at 297.0 K and C_2H_6 at 297.0 K on BPL Activated Carbon [21] Log–Log plot **e** C_2H_6 at 305.55 K and CO_2 at 305.95 K on NaX [8] Log–Log plot

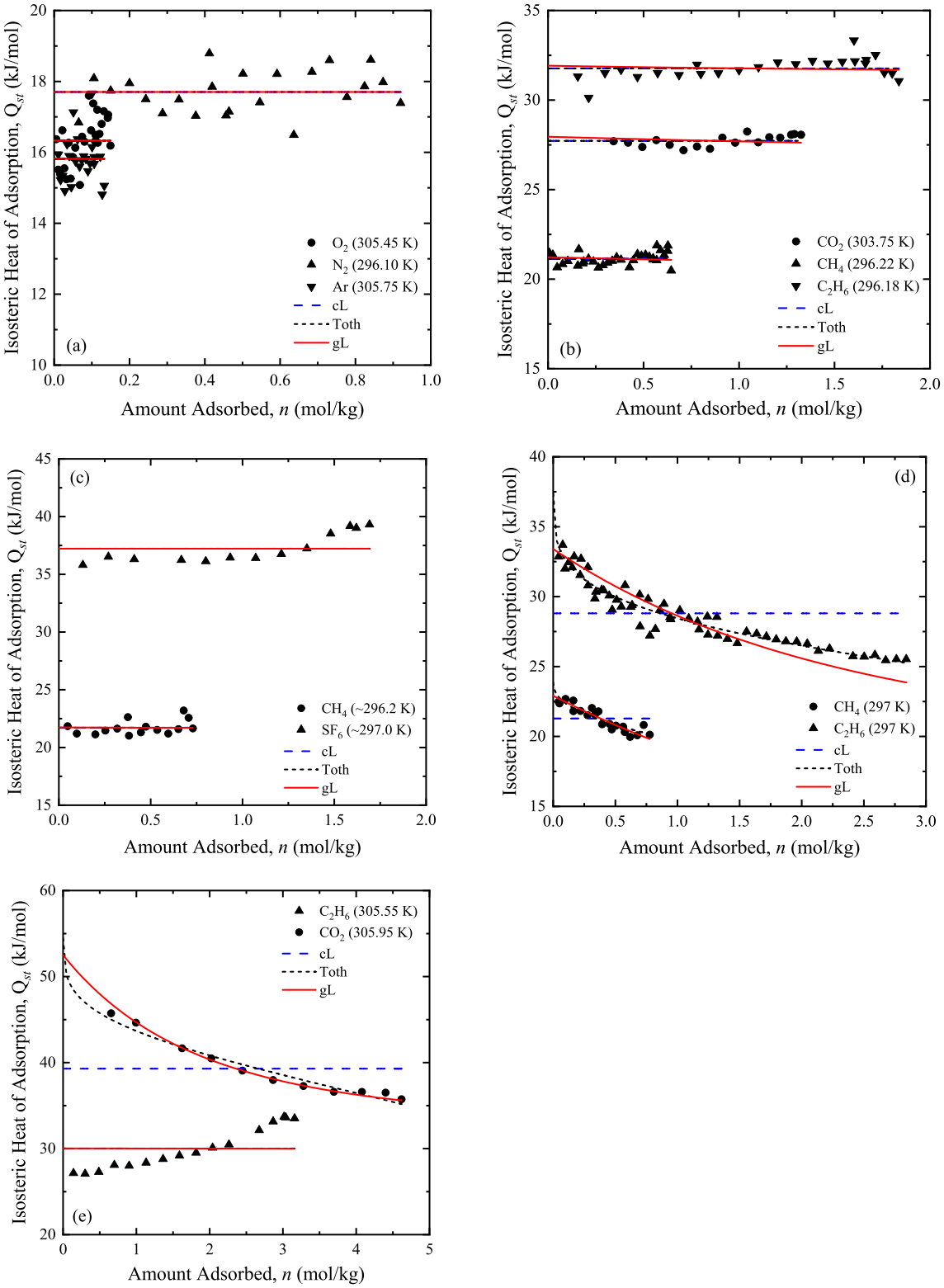

Fig. 6 Pure component isosteric heat of adsorption **a** O_2 at 305.45 K, N_2 at 296.10 K, and Ar at 305.75 K on Silicalite [6] **b** CO_2 at 303.75 K, CH_4 at 296.22 K, and C_2H_6 at 296.18 K on Silicalite [6] **c** CH_4 at 296.2 K and SF_6 at 297.0 K on Zeolite MFI [10] **d** CH_4 at 297.0 K and C_2H_6 at 297.0 K on BPL Activated Carbon [21] **e** C_2H_6 at 305.55 K and CO_2 at 305.95 K on NaX [8]

Table 4 Model results for binary mixed-gas adsorption equilibria

Adsorbent	Adsorbates	T (K)	P (bar)	IAST ARD%			gL ARD%			
				x_1'	Q_{st_1}	Q_{st_2}	B_{12}(K)*	x_1'	$Q_{st,1}$	$Q_{st,2}$
Nuxit-AL charcoal [2, 38]	$C_2H_4(1)$–$CH_4(2)$	293.10	0.992	1.04	–	–	−811.72	1.45	–	–
Silicalite [39]	$C_2H_6(1)$–$CH_4(2)$	298.44	0.361–0.764	1.96	2.05	1.31	−155.17	3.23	2.03	1.09
Zeolite MFI [10]	$SF_6(1)$–$CH_4(2)$	~294.56	0.113–0.634	3.61	4.12	3.89	−751.00	1.37	4.21	3.06
BPL activated carbon [21]	$CH_4(1)$–$C_2H_6(2)$	297.00	0.034–0.703	5.51	8.22	13.43	−1858.33	3.22	5.18	10.80
NaX [39]	$CO_2(1)$–$C_2H_6(2)$	302.09	0.302–1.069	25.87	16.26	4.00	−1107.56	12.93	3.91	3.67

*Standard deviations of B_{12} parameter are nearly zero

loading of CH_4 regardless of the bigger size of C_2H_6 over CH_4. Figure 6d shows that both Toth and gL reliably fit the experimental heat of adsorption data while the cL estimations, indicating constant isosteric heat of adsorption, deviate substantially.

NaX is another nonideal and energetically heterogeneous adsorbent. Figure 5e indicates that all three models reliably fit the C_2H_6 adsorption isotherm at 305.55 K on NaX. On the other hand, only Toth and gL accurately represent the experimental adsorption isotherm data of CO_2 adsorption at 305.95 K on NaX while cL significantly under-estimates the adsorption amounts at low pressures. As shown in Fig. 6e, all three models suggest constant heat of adsorption in the case of C_2H_6. As for CO_2, Toth and gL satisfactorily capture the trend that the isosteric heat of adsorption decreases with the loading, highlighting the adsorbent surface heterogeneity. In contrast, cL suggests a constant heat of adsorption that is inconsistent with the experimental data.

4.3 Isosteric heat of adsorption for binary mixed-gas adsorption

The binary mixed-gas adsorption systems investigated include (1) $C_2H_4(1)$–$CH_4(2)$ on Nuxit-AL charcoal at 293.10 K and 0.992 bar, [2, 38] (2) $C_2H_6(1)$–$CH_4(2)$ on Silicalite at 298.44 K and 0.361–0.764 bar [39], (3) $SF_6(1)$–$CH_4(2)$ on Zeolite MFI at ~ 294.56 K and 0.113–0.634 bar [10], (4) $CH_4(1)$–$C_2H_6(2)$ on BPL Activated Carbon at 297.0 K and 0.034–0.703 bar [21], and (5) $CO_2(1)$–$C_2H_6(2)$ on NaX at 302.09 K and 0.302–1.069 bar [39]. The model results of IAST and gL isotherm are compiled in Table 4. Note that the gL isotherm for pure component adsorption is used to compute the adsorption isotherm, integral enthalpy, and isosteric heat of adsorption in both the IAST and gL frameworks. This approach ensures the same pure component adsorption basis for both IAST and gL in computing the mixed-gas adsorption equilibria and the isosteric heat of adsorption. The gL pure component isotherm parameters are taken from Table 3. The following minimization objective function, Eq. (46), is used to identify the gL binary interaction parameter B_{12} from the experimentally measured adsorbed phase mole fractions.

$$Obj = \sum_{l=1}^{N} \left(\frac{x_l'^{calc} - x_l'^{expt}}{\sigma_{x_l'^{expt}}} \right)^2 \tag{46}$$

where N denotes the total number of data points, $x_l'^{expt}$ and $x_l'^{calc}$ indicate the experimental and calculated adsorbed phase mole fractions of adsorbate components, with vacant sites excluded. Set to 0.05, $\sigma_{x_l'^{expt}}$ denotes the standard deviation in experimental adsorbed phase mole fraction.

Figure 7a shows the parity plot for the experimental and calculated adsorbed phase C_2H_4 mole fraction of $C_2H_4(1)$–$CH_4(2)$ on Nuxit-AL charcoal at 0.992 bar. The estimated adsorbed phase mole fractions from both IAST and gL are consistent with the experimentally measured adsorbed phase mole fractions. With the gL binary interaction parameter regressed from the experimental adsorbed phase mole fractions, i.e., $B_{12} = -811.72$ K, Fig. 8 shows the isosteric heat of adsorption predictions for both adsorbate components as a function of gas phase mole fraction. The IAST and gL isosteric heat of adsorption predictions are further compared against the modified Dubinin isotherm results reported in the literature [2] due to the absence of experimental data. The gL isotherm results closely follow the trends of the modified Dubinin isotherm results.

Similarly, Fig. 7b and c show the parity plots for the experimental and calculated adsorbed phase mole fraction of $C_2H_6(1)$–$CH_4(2)$ on Silicalite at 298.44 K and $SF_6(1)$–$CH_4(2)$ on Zeolite MFI at ~ 294.56 K, respectively. They show that for $C_2H_6(1)$–$CH_4(2)$ on Silicalite, both IAST and gL accurately estimate the adsorbed phase mole fractions with the gL binary interaction parameter $B_{12} = -155.17$ K. In contrast, gL outperforms IAST for $SF_6(1)$–$CH_4(2)$ binary on Zeolite MFI with $B_{12} = -751.0$ K. Figure 9a and b show the corresponding parity plots for isosteric heat of adsorption. Both the IAST and gL predictions for isosteric heat of adsorption based on the binary mixed-gas adsorption equilibria data are consistent with the experimental data.

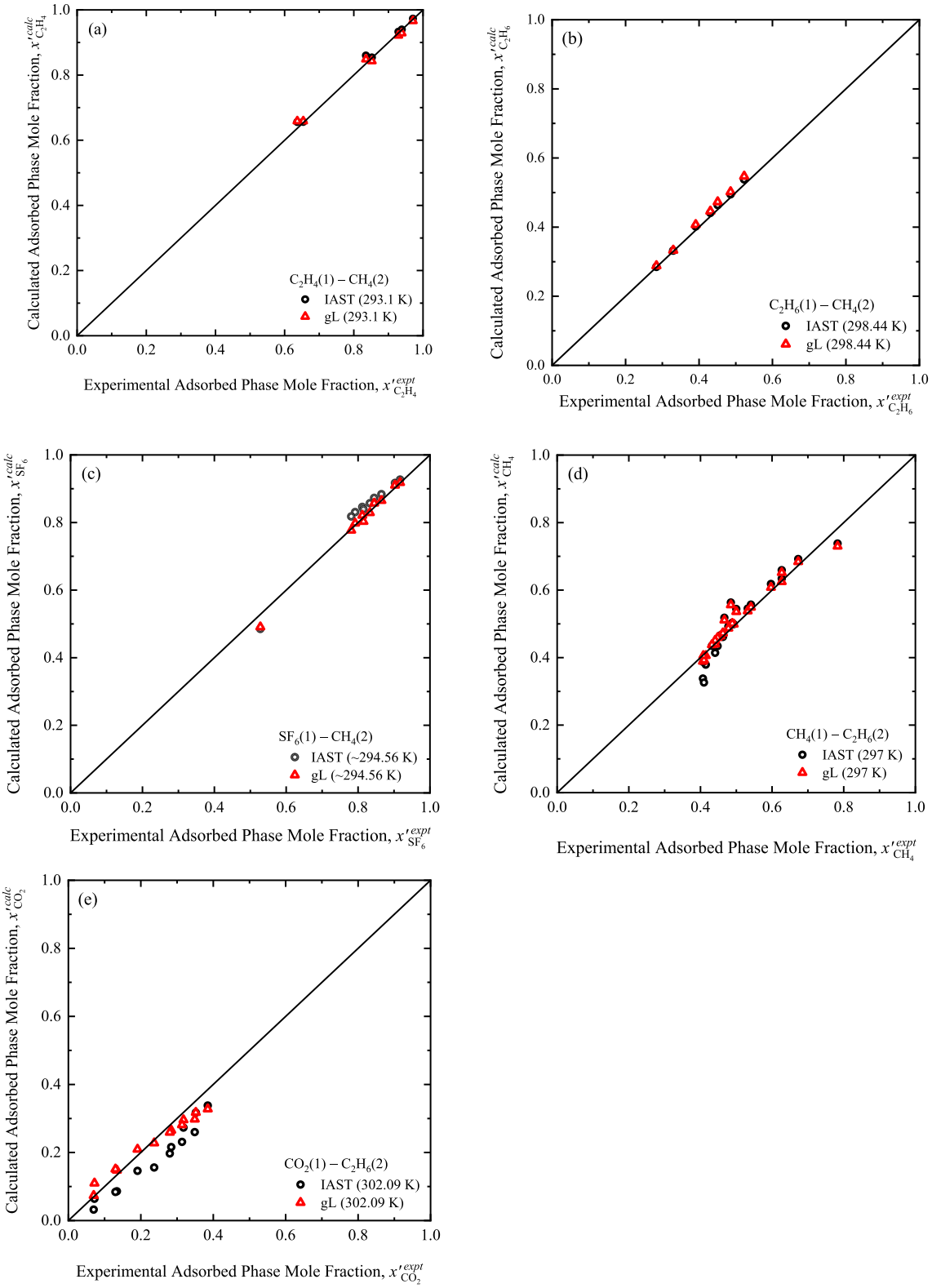

Fig. 7 Parity plots for adsorbed phase mole fraction of **a** $C_2H_4(1)$–$CH_4(2)$ on Nuxit-AL charcoal at 293.10 K and 0.992 bar [2, 38] **b** $C_2H_6(1)$–$CH_4(2)$ on Silicalite at 298.44 K and 0.361–0.764 bar [39] **c** $SF_6(1)$–$CH_4(2)$ on Zeolite MFI at ~ 294.56 K and 0.113–0.634 bar [10] **d** $CH_4(1)$–$C_2H_6(2)$ on BPL Activated Carbon at 297.0 K and 0.034–0.703 bar [21] **e** $CO_2(1)$–$C_2H_6(2)$ on NaX at 302.09 K and 0.302–1.069 bar [39]

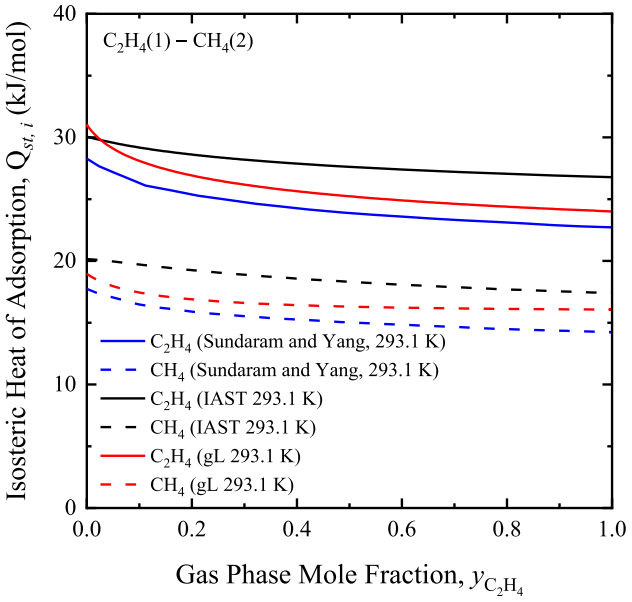

Fig. 8 Predicted isosteric heat of adsorption of $C_2H_4(1)$–$CH_4(2)$ on Nuxit-AL charcoal at 293.10 K and 0.992 bar [2, 38]

Figure 7d shows the parity plot for the experimental and calculated adsorbed phase CH_4 mole fraction of $CH_4(1)$–$C_2H_6(2)$ on BPL activated carbon at 297 K. With $B_{12} = -1858.33$ K, gL outperforms IAST with the estimated adsorbed phase mole fractions. Figure 9c shows the gL predictions for isosteric heat of adsorption are slightly better than the IAST predictions. The deviations from the experimental isosteric heat of adsorption data for C_2H_6 are likely related to the slightly inaccurate pure C_2H_6 isotherm data representation at the low pressure region shown in Fig. 5d. Interestingly, Tun [30] also investigated the same binary adsorption system of $CH_4(1)$–$C_2H_6(2)$ on BPL activated carbon at 297 K. He reported that Toth isotherm reliably fits the pure component adsorption isotherm in low pressures. However, the IAST results with Toth isotherm for pure component adsorption failed to estimate the mixed-gas adsorption equilibria and the isosteric heat of adsorption [30].

Figure 7e shows the parity plot for the experimental and calculated adsorbed phase CO_2 mole fraction of $CO_2(1)$–$C_2H_6(2)$ on NaX at 302.09 K. The parity plot indicates that the IAST predictions depart from the experimental data while gL reliably correlates the experimental adsorbed phase mole fraction with $B_{12} = -1107.56$ K. Figure 9d shows the isosteric heat of adsorption predictions from both IAST and gL. While the predictions for C_2H_6 from both models match the experimental data, the gL predictions for CO_2 are consistent with the data while the IAST predictions are considerably under-estimated.

We further examine the pressure dependence of isosteric heat of adsorption as predicted by IAST and gL. Three binary systems considered are $C_2H_6(1)$–$CH_4(2)$ on Silicalite at 298.44 K [39], $SF_6(1)$–$CH_4(2)$ on Zeolite MFI at ~ 294.56 K [10], and $CO_2(1)$–$C_2H_6(2)$ on NaX at 302.09 K [39], all at two different pressures, i.e., 0.1 bar and 5.0 bar. The mixed-gas adsorption equilibrium diagrams of above-mentioned systems are presented in Fig. S.1 of Supplementary Information while the isosteric heat of adsorption predictions are shown in Fig. 10. For the binary mixed-gas adsorption of $C_2H_6(1)$–$CH_4(2)$ on Silicalite, both the IAST and gL predictions at 0.1 bar and 5.0 bar show a constant isosteric heat of adsorption as shown in Fig. 10a. This homogenous adsorbent behavior can be explained with the weak adsorbate-adsorbent interaction i.e., $\tau_{i\phi} = \frac{B_{i\phi}}{T} \to 0$, as shown in Table 3, and the weak adsorbate–adsorbate interaction, i.e., $\tau_{12} = \frac{B_{12}}{T} \to 0$, as shown in Table 4. Similar behavior can be observed in the case of $SF_6(1)$–$CH_4(2)$ binary adsorption on Zeolite MFI at 0.1 bar highlighting the ideal adsorption behavior. However, Fig. 10b shows as the pressure is increased to 5.0 bar, the gL predictions for isosteric heat of adsorption suggest strong dependence of adsorbed phase composition. Although the pure component interaction parameters $B_{i\phi}$ are small as shown in Table 3, the binary interaction parameter, i.e., $B_{12} = -751.0$ K per Table 4, highlights strong nonideality in the adsorbed phase. In the case of $CO_2(1)$–$C_2H_6(2)$ binary system on NaX as shown in Fig. 10c, the gL predictions for CO_2 at both 0.1 bar and 5.0 bar show the isosteric heat of adsorption decreases as the adsorbed phase mole fraction of component $CO_2(1)$, x_1', increases. In contrast, the IAST predictions for CO_2 at 0.1 bar show that the isosteric heat of adsorption remains nearly constant and then decreases slightly as x_1' approaches unity. Then, at 5.0 bar, the IAST predictions suggest the isosteric heat of adsorption should increase with the increase in x_1'. These IAST predictions are not consistent with the expectation that stronger adsorption sites are preferred and therefore the heat of adsorption should decline with the increase in x_1'. Note that both gL and IAST give very similar predictions at 0.1 bar and 5.0 bar for the isosteric heat of adsorption of C_2H_6, indicative of ideal adsorption behavior for C_2H_6.

5 Conclusions

This work shows generalized Langmuir isotherm reliably represents the isosteric heat of adsorption for pure component adsorption with three model parameters: the intrinsic adsorption equilibrium constant, the heat of adsorption,

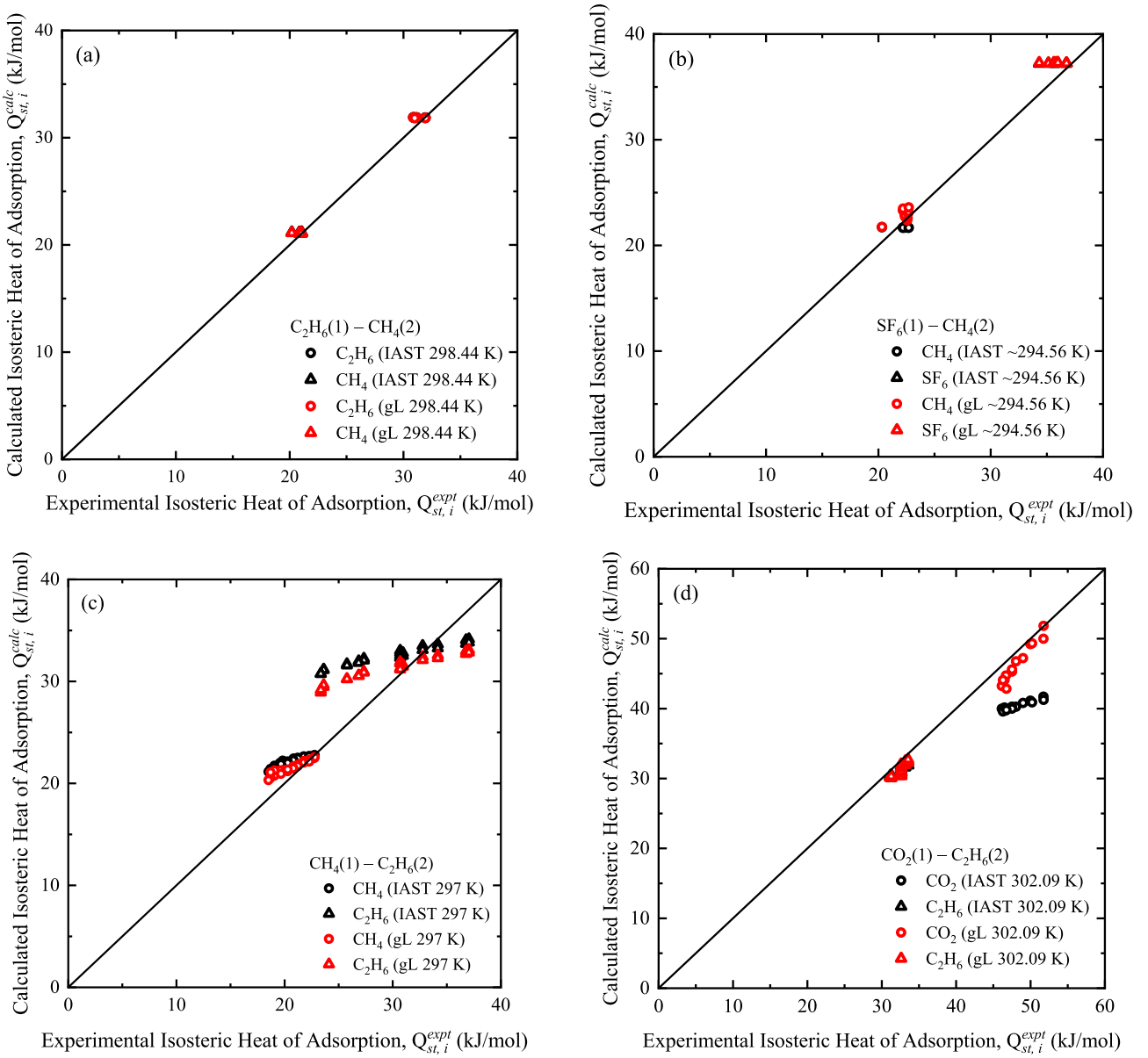

Fig. 9 Parity plots for isosteric heat of adsorption of **a** $C_2H_6(1)$–$CH_4(2)$ on Silicalite at 298.44 K and 0.361–0.764 bar [39] **b** $SF_6(1)$–$CH_4(2)$ on Zeolite MFI at ~ 294.56 K and 0.113–0.634 bar [10] **c** $CH_4(1)$–$C_2H_6(2)$ on BPL Activated Carbon at 297.0 K and 0.034–0.703 bar [21] **d** $CO_2(1)$–$C_2H_6(2)$ on NaX at 302.09 K and 0.302–1.069 bar [39]

and a binary adsorbate-adsorbent interaction parameter. Furthermore, generalized Langmuir reliably estimates the isosteric heat of adsorption as functions of surface loading and adsorbed phase composition with an additional binary adsorbate–adsorbate interaction parameter. Reliably representing both adsorption equilibria and isosteric heat of adsorption for multicomponent gas adsorption systems, the rigorous and robust generalized Langmuir isotherm is a powerful thermodynamic modeling tool to support simulation and design of industrial gas adsorption units.

Supplementary Information The online version contains supplementary material available at https://doi.org/10.1007/s10450-023-00379-x.

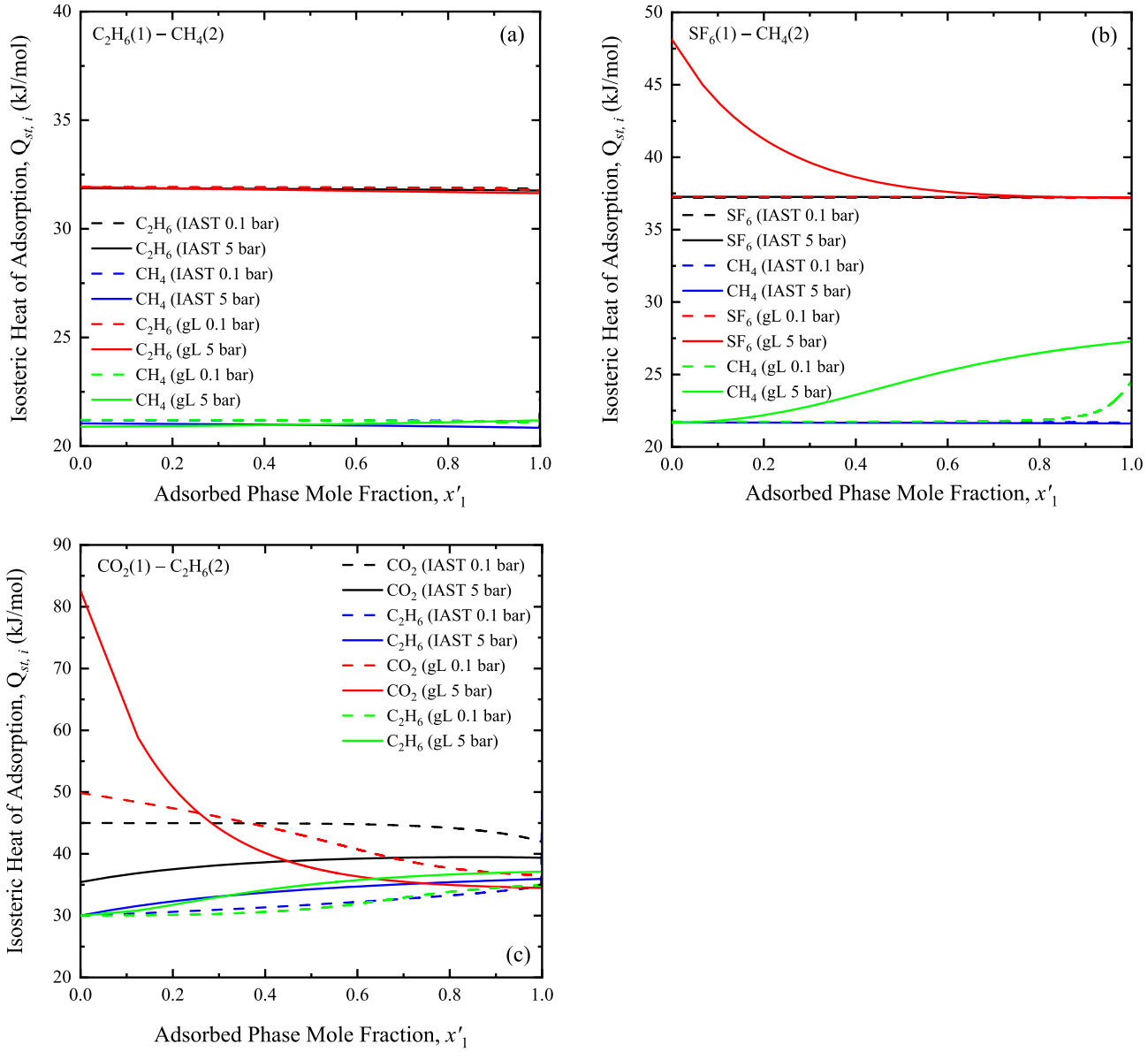

Fig. 10 Sensitivity analysis of isosteric heat of adsorption of **a** $C_2H_6(1)$–$CH_4(2)$ on Silicalite at 298.44 K [39] **b** $SF_6(1)$–$CH_4(2)$ on Zeolite MFI at ~ 294.56 K [10] **c** $CO_2(1)$–$C_2H_6(2)$ on NaX at 302.09 K [39]

Acknowledgements This report was prepared as an account of work sponsored by an agency of the United States Government. Neither the United States Government nor any agency thereof, nor any of their employees, makes any warranty, express or implied, or assumes any legal liability or responsibility for the accuracy, completeness, or usefulness of any information, apparatus, product, or process disclosed, or represents that its use would not infringe privately owned rights. Reference herein to any specific commercial product, process, or service by trade name, trademark, manufacturer, or otherwise does not necessarily constitute or imply its endorsement, recommendation, or favoring by the United States Government or any agency thereof. The views and opinions of authors expressed herein do not necessarily state or reflect those of the United States Government or any agency thereof.

Author contributions UH: conceptualization-equal, data curation-lead, formal analysis-lead, investigation-lead, methodology-equal, software-lead, validation-lead, visualization-lead, writing-original draft-lead. PV: conceptualization-supporting, data curation-supporting, formal analysis-supporting, methodology-supporting, writing-original draft-supporting. C-CC: conceptualization-equal, data curation-supporting, formal analysis-supporting, funding acquisition-lead, investigation-lead, methodology-equal, project administration-lead, resources-lead, software-supporting, supervision-lead, validation-equal, visualization-supporting, writing-original draft-supporting, writing-review & editing-lead.

Funding Funding support is provided by the U. S. Department of Energy under the grant DE-EE0007888. The authors gratefully acknowledge the financial support of the Jack Maddox Distinguished Engineering Chair Professorship in Sustainable Energy sponsored by the J.F Maddox Foundation.

Declarations

Competing interests The authors have no competing interests to declare that are relevant to the content of this article.

References

1. Yang, R.T.: Gas Separation by Adsorption Processes. Butterworth-Heinemann, Oxford (2013)
2. Sundaram, N., Yang, R.T.: Isosteric heats of adsorption from gas mixtures. J. Colloid Interface Sci. **198**(2), 378–388 (1998). https://doi.org/10.1006/jcis.1997.5300
3. Sees, M.D., Kirkes, T., Chen, C.-C.: A simple and practical process modeling methodology for pressure swing adsorption. Comput. Chem. Eng. **147**, 107235 (2021). https://doi.org/10.1016/j.compchemeng.2021.107235
4. Sircar, S.: Role of adsorbent heterogeneity on mixed gas adsorption. Ind. Eng. Chem. Res. **30**(5), 1032–1039 (1991). https://doi.org/10.1021/ie00053a027
5. Shen, D., Bülow, M., Siperstein, F., Engelhard, M., Myers, A.L.: Comparison of experimental techniques for measuring isosteric heat of adsorption. Adsorption **6**(4), 275–286 (2000)
6. Dunne, J.A., Mariwala, R., Rao, M., Sircar, S., Gorte, R.J., Myers, A.L.: Calorimetric heats of adsorption and adsorption isotherms. 1. O_2, N_2, Ar, CO_2, CH_4, C_2H_6, and SF_6 on Silicalite. Langmuir **12**(24), 5888–5895 (1996). https://doi.org/10.1021/la960495z
7. Sircar, S., Mohr, R., Ristic, C., Rao, M.B.: Isosteric heat of adsorption: theory and experiment. J. Phys. Chem. B **103**(31), 6539–6546 (1999). https://doi.org/10.1021/jp9903817
8. Dunne, J.A., Rao, M., Sircar, S., Gorte, R.J., Myers, A.L.: Calorimetric heats of adsorption and adsorption isotherms. 2. O_2, N_2, Ar, CO_2, CH_4, C_2H_6, and SF_6 on NaX, H-ZSM-5, and Na-ZSM-5 Zeolites. Langmuir **12**(24), 5896–5904 (1996). https://doi.org/10.1021/la960496r
9. Siperstein, F., Gorte, R.J., Myers, A.L.: Measurement of excess functions of binary gas mixtures adsorbed in zeolites by adsorption calorimetry. Adsorption **5**(2), 169–176 (1999). https://doi.org/10.1023/a:1008973409819
10. Siperstein, F., Gorte, R.J., Myers, A.L.: A new calorimeter for simultaneous measurements of loading and heats of adsorption from gaseous mixtures. Langmuir **15**(4), 1570–1576 (1999). https://doi.org/10.1021/la980946a
11. Sircar, S., Golden, T.C.: 110th Anniversary: comments on heterogeneity of practical adsorbents. Ind. Eng. Chem. Res. **58**(25), 10984–11002 (2019). https://doi.org/10.1021/acs.iecr.9b01025
12. Sircar, S.: Heat of adsorption on heterogeneous adsorbents. Appl. Surf. Sci. **252**(3), 647–653 (2005). https://doi.org/10.1016/j.apsusc.2005.02.082
13. Tun, H., Chen, C.-C.: Isosteric heat of adsorption from thermodynamic Langmuir isotherm. Adsorption **27**(6), 979–989 (2021). https://doi.org/10.1007/s10450-020-00296-3
14. Son, K.N., Cmarik, G.E., Knox, J.C., Weibel, J.A., Garimella, S.V.: Measurement and prediction of the heat of adsorption and equilibrium concentration of CO_2 on zeolite 13X. J. Chem. Eng. Data **63**(5), 1663–1674 (2018). https://doi.org/10.1021/acs.jced.8b00019
15. Langmuir, I.: The adsorption of gases on plane surfaces of glass, mica and platinum. J. Am. Chem. Soc. **40**(9), 1361–1403 (1918). https://doi.org/10.1021/ja02242a004
16. Mathias, P.M., Kumar, R., Moyer, J.D., et al.: Correlation of multicomponent gas adsorption by the dual-site Langmuir model. Application to nitrogen/oxygen adsorption on 5A-zeolite. Ind. Eng. Chem. Res. **35**(7), 2477–2483 (1996)
17. Toth, J.: State equation of the solid-gas interface layers. Acta Chim Hung. **69**, 311–328 (1971)
18. Chang, C.-K., Tun, H., Chen, C.-C.: An activity-based formulation for Langmuir adsorption isotherm. Adsorption **26**(3), 375–386 (2020). https://doi.org/10.1007/s10450-019-00185-4
19. Kaur, H., Tun, H., Sees, M., Chen, C.-C.: Local composition activity coefficient model for mixed-gas adsorption equilibria. Adsorption **25**(5), 951–964 (2019). https://doi.org/10.1007/s10450-019-00127-0
20. Sircar, S.: Excess properties and thermodynamics of multicomponent gas adsorption. J. Chem. Soc. Faraday Trans. **81**(7), 1527–1540 (1985). https://doi.org/10.1039/f19858101527
21. He, Y., Yun, J.H., Seaton, N.A.: Adsorption equilibrium of binary methane/ethane mixtures in BPL activated carbon: isotherms and calorimetric heats of adsorption. Langmuir **20**(16), 6668–6678 (2004). https://doi.org/10.1021/la036430v
22. Bulow, M., Lorenz, P.: Isosteric adsorption equilibria for binary krypton-xenon mixtures on CaA type zeolite. Ind. Eng. Chem. Res. **61**, 119–128 (1987)
23. Sircar, S.: Estimation of isosteric heats of adsorption of single gas and multicomponent gas-mixtures. Ind. Eng. Chem. Res. **31**(7), 1813–1819 (1992). https://doi.org/10.1021/ie00007a030
24. Myers, A.L., Prausnitz, J.M.: Thermodynamics of mixed-gas adsorption. AIChE J. **11**(1), 121–127 (1965). https://doi.org/10.1002/aic.690110125
25. Siperstein, F.R., Myers, A.L.: Mixed-gas adsorption. AIChE J. **47**(5), 1141–1159 (2001). https://doi.org/10.1002/aic.690470520
26. Sundaram, N.: A modification of the Dubinin isotherm. Langmuir **9**(6), 1568–1573 (2002). https://doi.org/10.1021/la00030a024
27. Hamid, U., Vyawahare, P., Tun, H., Chen, C.-C.: Generalization of thermodynamic Langmuir isotherm for mixed-gas adsorption equilibria. AIChE J. **68**(6), e17663 (2022). https://doi.org/10.1002/aic.17663
28. Builes, S., Sandler, S.I., Xiong, R.: Isosteric heats of gas and liquid adsorption. Langmuir **29**(33), 10416–10422 (2013). https://doi.org/10.1021/la401035p
29. Renon, H., Prausnitz, J.M.: Local compositions in thermodynamic excess functions for liquid mixtures. AIChE J. **14**(1), 135–144 (1968). https://doi.org/10.1002/aic.690140124
30. Tun, H.: Prediction of Mixed-Gas Adsorption Equilibria and Isosteric Heat of Adsorption from Its Pure Component Adsorption Isotherms. Texas Tech University, Lubbock (2020)
31. Britt, H.I., Luecke, R.H.: The estimation of parameters in nonlinear implicit models. Technometrics **15**(2), 233–247 (1973). https://doi.org/10.1080/00401706.1973.10489037
32. Cmarik, G., Son, K., Knox, J.: *Standard Isotherm Fit Information for Dry CO_2 on Sorbents for 4-Bed Molecular Sieve*. 2017. NASA/TM—2017–219847. December 2017.
33. Szepesy, L., Illes, V.: Adsorption of gases and gas mixtures, I. Acta Chim. Hung. **35**, 37–50 (1963)
34. Khvoshchev, S.S., Zverev, A.V.: Calorimetric study of NH_3 and CO_2 adsorption on synthetic faujasites with Ca^{2+}, Mg^{2+}, and La^{3+} cations. J. Colloid Interface Sci. **144**(2), 571–578 (1991). https://doi.org/10.1016/0021-9797(91)90422-5
35. Llewellyn, P.L., Maurin, G.: Gas adsorption microcalorimetry and modelling to characterise zeolites and related materials. Comptes Rendus Chimie. Mar-Apr **8**(3–4), 283–302 (2005). https://doi.org/10.1016/j.crci.2004.11.004
36. Sircar, S., Cao, D.V.: Heat of adsorption. Chem. Eng. Technol. **25**(10), 945–948 (2002). https://doi.org/10.1002/1521-4125(20021008)25:10%3c945::Aid-ceat945%3e3.0.Co;2-f
37. Cao, D.V., Sircar, S.: Heats of adsorption of pure SF_6 and CO_2 on silicalite pellets with alumina binder. Ind. Eng. Chem. Res. **40**(1), 156–162 (2001). https://doi.org/10.1021/ie000650b

38. Szepesy, L., Illes, V.: Adsorption of gases and gas mixtures, III. Acta Chim. Hung. **35**, 245–253 (1963)
39. Dunne, J.A., Rao, M., Sircar, S., Gorte, R.J., Myers, A.L.: Calorimetric heats of adsorption and adsorption isotherms. 3. Mixtures of CH_4 and C_2H_6 in Silicalite and Mixtures of CO_2 and C_2H_6 in NaX. Langmuir **13**(16), 4333–4341 (1997). https://doi.org/10.1021/la960984z
40. Sing, K.S.W.: Assessment of surface area by gas adsorption. In: Rouquerol, F., Rouquerol, J., Sing, K.S.W., Llewellyn, P., Maurin, G. (eds.) Adsorption by Powders and Porous Solids, pp. 237–268. Academic Press, Boca Raton (2014)
41. McClellan, A.L., Harnsberger, H.F.: Cross-sectional areas of molecules adsorbed on solid surfaces. J. Colloid Interface Sci. **23**(4), 577–599 (1967). https://doi.org/10.1016/0021-9797(67)90204-4
42. Livingston, H.K.: The cross-sectional areas of molecules adsorbed on solid surfaces. J. Colloid Sci. **4**(5), 447–458 (1949). https://doi.org/10.1016/0095-8522(49)90043-4